Platinum Ordered Porous Electrodes: Developing a Platform for Fundamental Electrochemical Characterization

Brandy Kinkead[1], Julia van Drunen,[2] Michael T. Y. Paul,[1] Katie Dowling,[1] Gregory Jerkiewicz,[2] Byron D. Gates[1*]

[1]Department of Chemistry and 4D LABS
Simon Fraser University
Burnaby, BC V5A1S6
[2]Department of Chemistry
Queen's University
Kingston, ON K7L3N6

*email: bgates@sfu.ca
Tel: (+1) 778-782-8066; Fax: (+1) 778-782-3765
URL: http://www.sfu.ca/chemistry/groups/gates/index.htm

Abstract

High surface area platinum electrodes with an ordered porous structure (Pt-OP electrodes) have been prepared and characterized by electrochemical methods. This study builds a foundation upon which we can seek an in-depth understanding of the limitations and design considerations to make efficient and stable Pt-OP electrodes for use in electrochemical applications. A set of Pt-OP electrodes were prepared by controlled electrodeposition of Pt through a self-assembled array of spherical particles and subsequent removal of the spherical templates by solvent extraction. The preparation method was shown to be reproducible and the resulting electrodes were found to have clean Pt surfaces and a large electrochemical surface area ($\boldsymbol{A}_{\mathrm{ecsa}}$) resulting from both the porous structure, as well as the nano- and micro- scale surface roughness. Additionally, the Pt-OP electrodes exhibit a surface area enhancement comparable to commercially available electrocatalysts. In summary, the Pt-OP electrodes prepared herein show properties of interest for both gaining fundamental insights into electrocatalytic processes and for use in applications that would benefit from enhanced electrochemical response.

Keywords: Electrocatalysis; Platinum; Inverse Opal; Cyclic Voltammetry; Electron Microscopy; X-ray Diffraction; Electrochemical Surface Area

Introduction

The preparation of platinum electrodes has attracted considerable interest over the last decade owing to its potential impact on a wide range of applications. Many of these require Pt electrodes with a high electrochemical surface area ($\boldsymbol{A}_{ecsa}$), where $\boldsymbol{A}_{ecsa}$ is the surface area of Pt in direct contact with electrolyte at which electrochemical reactions can take place. Moreover, maintaining a large $\boldsymbol{A}_{ecsa}$ while minimizing the device footprint is generally a must for high performance technologies [1-3]. This requires Pt electrodes with a large roughness factor (RF), defined as the ratio of the $\boldsymbol{A}_{ecsa}$ to the geometric area ($\boldsymbol{A}_{geom}$) occupied by the sample ($RF = \boldsymbol{A}_{ecsa}/\boldsymbol{A}_{geom}$) [3-5]. Such Pt electrodes are commonly used in electrochemical detection of a multitude of analytes, such as dissolved gases [6-7], glucose [8-9], or hydrogen peroxide [10]. In polymer electrolyte membrane fuel cells, Pt serves as an electrocatalyst at which reactions such as the oxidation of alcohols and hydrogen, or the reduction of oxygen occur [3, 11-13]. Further improvements are, however, necessary to design and prepare high RF Pt electrodes with optimized efficiency and stability, while decreasing the amount of required Pt, commonly referred to as Pt loading. This task necessitates a better understanding of how electrochemical reactions on Pt are affected by the defining characteristics of high surface area porous electrodes [1, 2, 11, 13]. The features of interest in this study include the design of porous electrodes (e.g., pore size and shape, interconnection between pores) and the structure of the Pt framework (e.g., grain size and surface topography).

Platinum electrodes with a large $\boldsymbol{A}_{ecsa}$ can be prepared by a number of methods. One approach is the synthesis and subsequent deposition of Pt nanoparticles onto an electronically conductive support, or the electrochemical or chemical deposition of Pt nanoparticles directly

onto the support material. The use of Pt nanoparticles produces a large $\boldsymbol{A}_{ecsa}$ for a relatively small Pt loading, but requires that the support and electrocatalyst-support interactions remain stable during electrochemical reactions [1, 14]. Another approach involves platinization of high surface area or sacrificial templates to produce Pt electrodes with a large $\boldsymbol{A}_{ecsa}$. This type of electrode is commonly achieved by either physical vapour deposition or electrodeposition techniques. Physical vapour deposition onto a high surface area support can produce large $\boldsymbol{A}_{ecsa}$ Pt electrodes, but is a directional technique and is, therefore, limited in its' ability to equally control the distribution of Pt over three dimensions [15-19]. Electrodeposition through a sacrificial template (e.g., lyotropic liquid crystals [20] or polycarbonate membranes [21-23]) is a versatile method for creating porous Pt electrodes with a variety of pore shapes, sizes, and interconnectivity without the need for a secondary support. Depending on the sacrificial template, such prepared Pt electrodes can have a large $\boldsymbol{A}_{ecsa}$. For our studies, we sought a structure and composition amenable to gaining a fundamental understanding on the effect of electrode morphology on the electrocatalytic behavior of Pt electrodes for applications in energy-generating and sensing devices.

Prior studies demonstrated the feasibility to prepare ordered porous electrodes via colloidal templates and their use in electrochemical applications [24-35]. They include the preparation of nickel ordered porous electrodes for use in alkaline water electrolysis [27], hierarchical Ge ordered porous electrodes for anodes in lithium-ion batteries [31], and Au and Pt ordered porous electrodes for the detection of dissolved glucose [30-32]. Platinum ordered porous and Pd modified Pt ordered porous electrodes were also prepared for applications in direct methanol fuel cells [33-36]. In this contribution, we report on the systematic preparation of pure Pt ordered porous (Pt-OP) electrodes (Figure 1) and their characterization using material

science and electrochemical techniques. The aim of this research is to develop a platform for the identification and quantification of the relationship between structure and electrocatalytic activity. Therefore, these electrodes were designed with a specific pore size, interconnectivity, and thickness. Our analysis also includes assessment of reproducibility in preparing these Pt-OP electrodes, as well as their electrochemical characteristics and long-term stability. It is expected that our long-term research efforts will allow us to fine-tune the porosity, pore structure, and thickness of Pt-OP electrodes for optimization of their electrocatalytic performance.

Experimental

The Pt-OP electrodes were built upon a suitable electronically conducting support that also serves as a platform for characterizing these porous materials. We demonstrated the principles described herein using a silicon wafer supported gold film (200 nm), with a 5-nm Cr adhesion layer in between the surface and support prepared *via* thermal evaporation in a Kurt J. Lesker physical vapour deposition (PVD 75) system. These substrates were fractured into approximately 1 cm × 2 cm rectangles. This support provided flat, conductive surfaces that did not interfere with electrochemical measurements of the Pt-OP electrodes. Polystyrene (PS) spheres with a hydrodynamic diameter of 460 nm (Polysciences, Inc.) were self-assembled at an air-water interface using an adaptation of a previously reported procedure [37]. In brief, PS spheres (1 wt% in 1-butanol) were drop cast onto the air-water interface of heated (~40°C), freshly deionized water (18.2 MΩ cm). Drops of solution containing PS spheres were added until the droplets no longer dispersed across this interface. The resulting assemblies of PS spheres were transferred onto the conductive support (after rinsing the support with ethanol) by a

dip coating process. Multiple layers of PS sphere were assembled onto these supports by repeated dip coating. Such assembled layers of close-packed PS spheres were dried overnight in a vacuum desiccator and, subsequently, rinsed with ethanol to remove any residual butanol from the self-assembly process. Platinum electrodeposition was accomplished by potential cycling of the gold substrate between -0.18 and 1.20 V vs. Ag/AgCl at a potential scan rate of 175 mV s^{-1} [35]. The aqueous electrodeposition solution contained 5mM of H_2PtCl_6 (Sigma Aldrich, ACS Grade), 0.2 M of H_2SO_4 (Fisher Scientific, ACS Grade) and ~35mM of polyvinylpyrrolidone (Sigma Aldrich, 55k MW), which acted to improve uniformity of the Pt deposit within the sacrificial PS template [38]. After Pt electrodeposition, the PS template was removed by Soxhlet extraction with refluxing toluene for at least 4 h. Extracted porous electrodes were immersed and sonicated in first a solution of acetone and then a solution of isopropanol to remove traces of organic material originating from the preparation of the electrode. The geometric area ($\boldsymbol{A}_{geom}$) of the prepared electrodes was determined by photographing the electrodes on grid paper (Figure 2d) and evaluating the area occupied by the electrode with ImageJ 1.45s software.

The solvent washed Pt-OP electrodes were imaged by scanning electron microscopy (SEM) using a Strata DB235 FESEM/FIB to evaluate thickness, pore shape and size, and long-range order within the Pt-OP electrodes. X-ray diffraction (XRD) analysis was performed using a Rigaku Rapid-Axis Diffractometer with a Cu Kα1 radiation source (λ = 1.5406 Å) to examine the grain size of Pt crystallites within Pt-OP electrodes. Platinum mass loading was evaluated by flame atomic absorption spectroscopy (FAAS) using an Aurora Biomed TRACE AI1200 spectrometer equipped with a Pt hollow cathode lamp. After electrochemical examination, each Pt-OP electrode was digested in a solution of aqua regia for FAAS analysis. The aqua regia solution was prepared from a 3:1 (v/v) solution of hydrochloric acid (36.5 – 38.0% in water;

Anachemia Canada, Inc., Richmond, BC, Canada) and nitric acid (68 – 70% in water; Anachemia Canada, Inc., Richmond, BC, Canada). *CAUTION: Aqua regia solutions are extremely corrosive. This solution should be handled with extreme care.*

Electrochemical measurements were carried out using a Princeton Applied Research model 263A potentiostat with a Pt reversible hydrogen electrode (RHE) as a reference electrode and Pt gauze with electrodeposited Pt black as a counter electrode. All electrodes and the custom-made electrochemical cell used in this study were prepared by Verrerie de Precision Enr. Platinum electrode materials were supplied by Alfa Aesar (Pt ≥ 99.9%). Glassware, counter and reference electrodes were cleaned by established methods prior to use [39-40]. Before each electrochemical experiment, working electrodes were refluxed in isopropanol to remove organic surface residues. High purity N_2 gas (Praxair, 99.998%) was bubbled through the electrolyte to expel any reactive gases prior to electrochemical measurements. The Pt-OP electrodes were characterized using cyclic voltammetry (CV) in 0.1 or 0.2 M aqueous H_2SO_4 solution (Fisher Scientific, ACS Grade) prepared with high purity water (18.2 MΩ cm). Cyclic voltammetry profiles over a potential region of 0.05 to 1.25 V vs. RHE encompass the region of underpotential deposition of hydrogen (H_{UPD}) and oxide formation and reduction [41-42]. Because CV features in this potential range are sensitive to trace amounts of impurities and the surface orientation of the Pt electrode, this CV analysis allowed us to evaluate the purity of the system and to identify any preferential Pt grain orientation. The $\boldsymbol{A}_{ecsa}$ of the Pt-OP electrodes was determined by integrating the H_{UPD} (~0.05 – 0.45 V vs. RHE) and dividing this by the charge density (~0.05 – 0.45 V) of 210 μC cm^{-2}, which corresponds to the adsorption of a monolayer of H_{UPD} [4, 43].

Results and Discussion

A series of electrodes with different thicknesses were made in order to systematically evaluate their three-dimensional interconnectivity, stability and electrochemical characteristics. All samples were made in triplicate to evaluate the reproducibility of the preparation methods and their electrochemical responses. A terminology was developed to describe the Pt-OP samples, corresponding to the approximate thickness of the Pt deposit within the sacrificial template of PS spheres (Figure 1). For example, a "type 1/3" Pt electrode contains a uniform deposit with a thickness of ~1/3 the height of a single PS sphere in a close packed arrangement. Due to the thickness of the deposit, the "type 1/3" structure is non-porous and simply presents an electrode with a designed roughness. A "type 3/4" sample corresponds to uniform Pt deposit with a thickness equivalent to ~3/4 the height of a PS sphere in a close packed arrangement. The three dimensional (3D) porous structure of the "type 3/4" electrode contains interconnecting pores with circular openings on top. A "type 1¾" sample corresponds to uniform Pt deposit with a thickness equivalent to ~7/4 of the height of a single PS sphere in the prepared template. The 3D porous structure of the "type 1¾" electrode contains two porous layers. The first layer consists of interconnected spherical pores. The second layer contains interconnected pores with circular openings on top. The first and second layers are also interconnected, thus facilitating both vertical and horizontal penetration and diffusion by a fluid. This series of samples were chosen in order to evaluate diffusion of electrochemically active species within the porous structure as a function of dramatic changes in RF between the sample types, as well as to demonstrate the modularity and reproducibility of this method of preparing 3D Pt-OP electrodes.

Dimensions and film morphology of each electrode were evaluated by SEM analysis, and typical images from this inspection are presented in Figure 2. The pore size formed by selective

removal of the spherical PS templates was determined by measuring the distance between the middle of two adjacent, connected pores (SI Figure 1). Several measurements were taken and an average pore diameter was found to be 444 ± 16 nm. It is important to add that the pore size can be controlled by varying the diameter of the spherical PS particles assembled in the sacrificial template. The focus of this study is, however, on the systematic comparison of varying thickness and porosity of Pt electrodes with a well-defined pore shape, size and connectivity. Our results shown in Figure 2 demonstrate that our PS sphere templates are non-perfect and contain structural defects. In some regions, we observe a perfect hexagonal close-packed arrangement with each PS sphere having a point contact with 6 others. In other regions there are, however, spheres in contact with fewer neighbouring spheres. A lack of contact with neighbouring spheres can result in a lack of interconnectivity, which can translate into a decrease in RF and limitations in the horizontal fluid flow between adjacent pores. The interconnection size (the degree of overlap of adjacent PS spheres) is generally determined by the hardness and degree of close packing of the spherical PS templates [46]. The average diameter of the circular interconnection between adjacent pores in our Pt-OP electrodes was found to be 120 ± 10 nm, as determined from cross-sectional SEM measurements of openings between adjacent pores (SI Figure 1). This interconnection size could limit penetration of the electrolyte into underlying porous layers, which is considered later in our discussion. To evaluate bulk interconnectivity we have counted the number of pores in an as-prepared single layer electrode (e.g., the number of pores per cm^2) and compared it to the theoretical number of pores per cm^2 for a homogeneously close-packed single layer structure. From this comparison, we have determined that <4% of spheres were missing from the total number of spheres that could be assembled into a single layer with a hexagonal close packed structure. Based on this information, further improvements

to the assembly of PS spheres could only increase the observed RF by <4%. Furthermore, the interconnectivity was evaluated by counting the average number of neighboring pores connected to an individual pore (as visible in SEM imaging). In a uniformly close-packed structure of assembled PS spheres each pore is connected to six adjacent pores arranged in a hexagonal array within the OP electrode. For our samples, we found that each pore in the Pt-OP electrodes is, on average, connected to four adjacent spherical pores. Therefore, these structures have a considerably high density of connected pores and we believe that horizontal fluid flow should not be significantly limited. Overall, the OP-electrodes were determined to have suitable pore sizes, density and connectivity for our electrochemical studies.

We analyzed the electrochemical characteristics of Pt-OP electrodes by recording CV profiles in the potential range corresponding to H_{UPD} adsorption and desorption [41], and PtO formation and reduction [42]. Figure 3a shows CV profiles for a Pt-OP electrode in 0.1 M H_2SO_4 recorded at a scan rate (s) of 25 mV s^{-1} that is representative of the overall trend observed in 500 transients. The initial scan contains ill-defined peaks in both the H_{UPD} region (0.05 – 0.4 V vs. RHE) and PtO region (0.7 – 1.25 V vs. RHE). The initial shape of the CV profile in the oxide formation region is characteristic of carbon based contamination on the Pt-OP electrode that undergoes oxidative desorption upon prolonged potential cycling [39]. After 30 cycles the CV features corresponding to H_{UPD} adsorption and desorption, as well as PtO formation and reduction, are well-defined and characteristic of an impurity-free system. Further potential cycling (100, 250 and 500 cycles) does not change the shape of the CV features, but decreases their current density values. This observation indicates that there are no structural changes in the Pt deposit, but that $\boldsymbol{A}_{ecsa}$ is gradually reduced. Integration of the CV features corresponding to H_{UPD} adsorption allows us to determine $\boldsymbol{A}_{ecsa}$ as a function of the cycle number (Figure 3b) [40].

An analysis of the $\boldsymbol{A}_{ecsa}$ values demonstrates a gradual decrease of $\boldsymbol{A}_{ecsa}$ up to nearly 40%. The decrease in $\boldsymbol{A}_{ecsa}$ may be assigned either to surface restructuring of Pt-OP or Pt electro-dissolution [44]. However, CV experiments alone do not allow us to distinguish the process responsible for $\boldsymbol{A}_{ecsa}$ loss and complementary measurements are necessary.

To better identify the phenomena responsible for the loss of $\boldsymbol{A}_{ecsa}$ we removed the Pt-OP electrodes from the electrolyte solution, rinsed with high purity water and analyzed these samples by both XRD (Figure 3c and 3d) and SEM (Figures 3e to 3g). We monitored changes in the full-width-at-half maximum of the XRD peak corresponding to Pt (111) and used this value to calculate the grain size of Pt using the Scherrer formula [48]. The results demonstrate that the average grain size gradually increases upon potential cycling by up to 35% (Figure 3d). Additionally, this change occurs in good correspondence with the observed loss in $\boldsymbol{A}_{ecsa}$ (Figure 3b). Analysis of the Pt-OP electrodes by SEM reveals corresponding changes in morphology. The Pt-OP deposits initially have spherically shaped openings with smooth Pt walls (Figure 3e). Scanning electron microscopy examinations of these porous electrodes after CV analysis indicate a change to both the texture and shape of the pores. After 100 cycles the walls separating spherical pores become thinner and the shape less spherical (Figure 3f). These changes are even more pronounced after ~500 cycles (Figure 3g). In addition, potential cycling of Pt-OP for a total of 500 times leads to further thinning of the walls and generates vertical cracks between pores. The observed changes in SEM can be quantified by measuring changes in the area of the upper pore opening (leading into the Pt-OP electrodes) observed by SEM without tilting the stage (SI Figure 1). This analysis reveals that the average upper pore opening increased from $1.16 \pm 0.02 \times 10^5$ nm^2 with no cycling, to $1.40 \pm 0.08 \times 10^5$ nm^2 after 100 cycles, and to $1.57 \pm 0.04 \times 10^5$ nm^2 after 500 cycles. Altogether, the CV, XRD, and SEM results allow us to

conclude that the loss in $\boldsymbol{A}_{ecsa}$ is most likely due to Pt electro-dissolution. We hypothesize that the outermost layer of Pt is dissolving from the surfaces of the Pt-OP electrodes, and that the outermost layer is composed of Pt with a grain size smaller than that of the underlying layers of Pt. This outer layer of Pt is also most likely less dense and, therefore, more porous than the underlying layers. Removal of the outermost layers of Pt from the Pt-OP electrodes would thus expose a dense, underlying film of Pt composed of larger Pt grains, as well as a more stable $\boldsymbol{A}_{ecsa}$ and electrochemical response [45]. In later studies, it will be important to examine whether electro-dissolution of Pt-OP is uniform throughout the porous structure and to evaluate methods for reducing Pt loss, such as thermal annealing to induce grain growth within the Pt electrode before electrochemical testing.

A systematic study was performed to compare three different types of Pt-OP electrodes. As depicted in Figure 1, these three electrodes were films of type 1/3, 3/4, and 1¾. In Figure 4a, we present three representative CV profiles for the three types of Pt-OP electrodes after reaching a point at which the respective CV profiles do not change significantly (typically after 200 cycles). These CV profiles have been normalized by their measured geometric surface area ($\boldsymbol{A}_{geom}$) as described in the experimental section. Similar to that observed for the Pt-OP electrode described above, CV profiles underwent transformations with continued cycling corresponding to the initial removal of surface contaminants followed by Pt dissolution from the outermost surfaces containing small grain size and low density Pt. The CV profiles demonstrate that all three systems are impurity-free (after initial cycling to remove carbon based surface contaminants) and again the features for H_{UPD} adsorption and desorption can be used to determine $\boldsymbol{A}_{ecsa}$. Triplicates of each sample type were prepared and analyzed in the same manner for a statistical comparison of the results reported on these structures. Figure 4b presents the

experimental RF ($RF_{exp} = \boldsymbol{A}_{ecsa} / \boldsymbol{A}_{geom}$) values for the three types of Pt electrodes and reveals that RF_{exp} increases with increased OP thickness and thus with the Pt loading. The RF_{exp} values were 18.3 ± 1.9, 24.9 ± 0.5, and 30.3 ± 1.0 for type 1/3, 3/4, and 1¾ samples, respectively. The Pt-OP electrodes were prepared reproducibly as indicated by the relatively small error bars associated with each type of electrode. The progressive increase in RF_{exp} with sample thickness provides evidence that the electrolyte can traverse the open pore structure through the ~120 nm diameter interconnects. As mentioned earlier, the interconnectivity of these porous electrodes—as determined by their dimensions, overlap of the spherical templates, and thickness of the electrode—could limit vertical and horizontal transport within these materials. These are variables that could be analyzed in the future using similar Pt-OP electrodes, but are beyond the current study of developing and characterizing these electrodes as a platform for further fundamental studies.

The controlled porous nature of the Pt-OP electrodes is an essential factor for achieving a platform for further fundamental electrochemical studies. The structure of and connection between the pores of the Pt-OP electrodes help to define the RF_{exp} for each type of electrode. The reported RF_{exp} in Figure 4 was determined by dividing the measured $\boldsymbol{A}_{ecsa}$ by the two dimensional area of the electrode covered by these Pt-OP structures ($\boldsymbol{A}_{geom}$). To better evaluate the micro- and nano- roughness of the Pt surfaces within the porous structure, it is necessary to consider the geometric surface area within the Pt-OP electrodes formed by the network of interconnected pores ($\boldsymbol{A}_{pore\text{-}geom}$); where $\boldsymbol{A}_{pore\text{-}geom}$ is a theoretical representation of the porous structures, lacking micro, or nano- pore surface roughness. The $\boldsymbol{A}_{pore\text{-}geom}$ has been estimated (Equation 1) by evaluating the average pore radius (r_{pore}), density of the pores (ρ_{pore}, pores per cm^2), and average thickness of the electrochemically deposited Pt electrode ($t_{electrode}$), as

measured by the number of porous layers (e.g., $t_{electrode}$ is 1/3 for sample type 1/3), from SEM analysis.

$$\boldsymbol{A}_{pore\text{-}geom} = 4\pi(r_{pore})^2 \times \rho_{pore} \times t_{electrode} \qquad \text{(Eq. 1)}$$

Average pore density within the Pt-OP samples was determined to be $4.91 \pm 0.02 \times 10^8$ pores per cm^2. For the sample type 1¾, the pore density is assumed to be double that for the single layer structures as a function of our assembly method. We were unable to accurately determine the pore density of the bottom layer within these Pt-OP electrodes by SEM as it is covered by a continuous top layer of porous Pt. If the Pt electrodes have no micro- or nano-surface roughness, then we would expect the theoretical roughness factor ($RF_{pore\text{-}geom}$ or $\boldsymbol{A}_{pore\text{-}geom}/\boldsymbol{A}_{geom}$) to be similar to RF_{exp}. Using the method described above, $RF_{pore\text{-}geom}$ was calculated to be 1.02 ± 0.01, 2.29 ± 0.01, and 5.34 ± 0.02 for sample type 1/3, 3/4, and 1¾, respectively. We also determined the real surface roughness (RF_{real}) – defined as $\boldsymbol{A}_{ecsa}/\boldsymbol{A}_{pore\text{-}geom}$ – that is correlated with the micro- and nano- scale surface roughness of the Pt surfaces within the Pt-OP electrodes (Table 1). If the surfaces of the porous electrodes were atomically smooth, and if all Pt surfaces were in contact with the electrolyte, RF_{real} would be equivalent to a value of 1. For our Pt-OP electrodes, the average RF_{real} was 11.4, demonstrating that micro- and nano-roughness of the Pt surfaces within the porous structure contributes significantly to the total $\boldsymbol{A}_{ecsa}$. In addition, the RF_{real} decreases with increasing thickness of the Pt-OP electrodes from 17.6 ± 1.9 for sample type 1/3, to 10.9 ± 0.4 for sample type 3/4, and 5.6 ± 0.2 for sample type 1¾. This trend agrees with observations made in the structural and electrochemical analyses by SEM and CV of the Pt-OP electrodes. For example, the analysis by SEM of sample type 1/3 electrodes indicates that they are largely composed of a thin, roughened Pt film (lacking any well-defined 3D porous structure). Moreover, the sample type 1/3 electrodes have a comparable

RF_{exp} to that of a Pt electrodeposited film prepared without the use of the sacrificial PS templates. Thin Pt electrodes derived without the use of a sacrificial template displayed RF_{exp} values ranging between 12 and 17, depending on the Pt loading. This comparison suggests that the outermost surfaces of electrodeposited Pt have high surface roughness, but that Pt deposited against the spherical PS templates is comparably smooth. Therefore, future studies could greatly enhance the $\boldsymbol{A}_{ecsa}$ by producing roughened Pt surfaces within the spherical pores of thick Pt-OP electrodes.

We prepared a thicker Pt-OP electrode to further explore the trend of electrochemical enhancement as it correlates with Pt-OP electrode thickness. This analysis also demonstrated the utility of our methods to make customized Pt-OP electrodes. For this study, we prepared a 3 layer Pt-OP electrode. These samples, referred to as a sample type 3, were characterized by SEM and CV analysis (Figure 5). The relatively thick Pt-OP electrodes contain cracks, as seen in the SEM images, which most likely develop due to relaxation of strain within the samples upon removal of the PS templates [47]. These cracks are not regarded as detrimental to the functionality of the porous electrode, and could increase the porosity of, and thus accessibility of electrolyte into, these structures. The shape of the CV profiles for this thicker sample is comparable to the other Pt-OP electrodes, indicating relatively clean Pt surfaces. This sample exhibited an RF_{exp} of 55 ± 0.1 after stabilization of the CV profiles, which is approximately twice that of the value measured for sample type 1¾ electrodes. A comparison of this enhancement factor to that observed for the other sample types suggests that the cracks within these Pt-OP electrodes do not add significantly to the measured $\boldsymbol{A}_{ecsa}$. The Pt mass per $\boldsymbol{A}_{geom}$ of the sample type 3 was determined by FAAS to be 340 ± 60 μg Pt per cm^2. The ratio of $\boldsymbol{A}_{ecsa}$ to Pt mass for this sample is 16.2 m^2 per gram of Pt. Interestingly, this value of $\boldsymbol{A}_{ecsa}$ per gram of Pt

is well within the range of those reported by 3M for their nanostructured thin film (NSTF) catalyst layers used for oxygen reduction reaction (ORR) electrocatalysis (e.g., from 5 to 17 m^2 per gram of Pt) [15]. In addition, our 3 layer Pt-OP electrode is comparable to previous reports on relatively thick, ordered porous Pt. For example, the preparation of a Pt-OP electrode using a template of silica spheres produced an electrode with a roughness factor of nearly 60 for a Pt mass of 532 µg per cm^2 ($\boldsymbol{A}_{geom}$) [35]. This yields a surface area enhancement of 11.3 m^2 ($\boldsymbol{A}_{ecsa}$) per gram of Pt, which is comparable to the values observed for our samples. Variance between our results and those previously published are most likely the result of differences in electrode thickness, Pt surface roughness, and template sphere size. The potential use of Pt-OP electrodes as electrocatalysts is demonstrated in part by their comparable surface area enhancement with current catalysts layers being pursued for industrial applications.

Conclusions

Platinum ordered porous (Pt-OP) electrodes were reproducibly prepared and characterized by electrochemical techniques. These ordered electrodes serve as a reproducible platform for evaluating the efficiency and stability of electrochemical processes that are relevant to understanding the dynamics and optimization of Pt electrocatalysis. The Pt-OP electrodes contained pores with regular dimensions, shapes, and connectivity, in addition to a well-defined thickness and roughness of the Pt surfaces. The Pt-OP electrodes are made by electrodeposition of Pt within a sacrificial template of self-assembled polystyrene spheres, followed by the selective removal of this polymer with toluene. A series of electrodes with specific pore sizes, interconnectivity, and thickness were prepared in order to evaluate their electrochemical

performance as a function of changes in the Pt-OP electrode thickness. These Pt-OP electrodes were characterized by electron microscopy (EM), X-ray diffraction (XRD) and cyclic voltammetry (CV) to evaluate the relationship between structure and electrochemical activity of these materials. The electrochemically active surface area ($\boldsymbol{A}_{ecsa}$) is reproducibly modified as a function of thickness of the porous electrodes. The micro- and nano- scale roughness of the Pt-OP electrodes was estimated by comparing the measured $\boldsymbol{A}_{ecsa}$ to the expected $\boldsymbol{A}_{ecsa}$ based on morphology of the porous electrodes. This comparative analysis demonstrated that micro- and nano- roughness of the Pt surfaces within the Pt-OP electrodes contributes significantly to the measured $\boldsymbol{A}_{ecsa}$. The combined results of the CV, XRD, and EM analyses suggest that the surface roughness of the Pt-OP electrodes is non-uniform. The inside of the spherical pores were smooth relative to the top surfaces of the electrodeposited platinum. The regularity of the Pt-OP electrodes was an essential component of also evaluating changes to the electrode surfaces as a function of sequential CV analyses. The prepared electrodes have comparable electrochemical activity to other porous platinum electrodes demonstrated in the literature. In fact, a Pt-OP electrode composed of three layers of interconnected spherical pores and a nominal diameter of ~444 nm have a comparable $\boldsymbol{A}_{ecsa}$ per gram to electrodes being pursued for the commercial application of low temperature fuel cells. The Pt-OP electrodes described in this study could have further applications in optimizing the efficiency and monitoring the long-term stability of Pt in these and other electrocatalytic applications.

Acknowledgements

This work was supported in part by the Natural Sciences and Engineering Research Council (NSERC) of Canada, the Canada Research Chairs Program (B.D. Gates), and the

Simons Foundation. This work made use of 4D LABS shared facilities supported by the Canada Foundation for Innovation (CFI), British Columbia Knowledge Development Fund (BCKDF), Western Economic Diversification Canada, and Simon Fraser University. We would like to thank Dr. Dev Sharma and Paul Mulyk for their assistance with FAAS measurements.

References

1. A. Kloke, F. von Stetten, R. Zengerle, S. Kerzenmacher, Adv. Mater. 23, 4976 (2011)
2. J. Zhang, C. M. Li, Chem. Soc. Rev. 41, 7016 (2012)
3. B. C. H. Steele, A. Heinzel, Nature 414, 345 (2001)
4. D. Chen et al., Electrocatalysis 2, 207 (2011)
5. C. M. Li, Chem. Soc. Rev. 41, 7016 (2012)
6. Y. J. Lee, J. Y. Park, J. Korean Phys. Soc. 58, 1505 (2011)
7. G. Korotcenkov, S. Do Han, J. R. Stetter, Chem. Rev. 109, 1402 (2009)
8. Y.-Y. Song, D. Zhang, W. Gao, X.-H. Xia, Chem.--Eur. J. 11, 2177 (2005)
9. J. H. Yuan, K. Wang, X. H. Xia, Adv. Func. Mater. 15, 803 (2005)
10. S. A. G. Evans et al., Anal. Chem. 74, 1322 (2002)
11. D.-J. Guo, Y. Ding, Electroanalysis 24, 2035 (2012)
12. E. Antolini, T. Lopes, E. R. Gonzalez, J. Alloys Compd. 461, 253 (2008)
13. M. K. Debe, Nature 486, 43 (2012)
14. J. D. Aiken III, R. G. Finke, J. Mol. Catal. A: Chem. 145, 1 (1999)
15. M. K. Debe, ECS Trans. 45, 47 (2012)
16. R. Giorgi et al., J. Fuel Cell Sci. Tech. 8 (2011)

17. A. Bonakdarpour, M. D. Fleischauer, M. J. Brett, J. R. Dahn, Appl. Catal. A. 349, 110 (2008)
18. B. E. Hayden, D. Pletcher, J. P. Suchsland, L. J. Williams, PCCP 11, 9141 (2009)
19. C. Guizard, A. Princivalle, Catal. Today 146, 367 (2009)
20. G. S. Attard, C. G. Goltner, J. M. Corker, S. Henke, R. H. Templer, Angewandte Chemie-Int. Ed. 36, 1315 (1997)
21. S. S. Mahshid, S. Mahshid, A. Dolati, M. Ghorbani, L. X. Yang, S. L. Luo, Q. Y. Cai, Electrochimica Acta 58, 551 (2011)
22. S. M. Choi, J. H. Kim, J. Y. Jung, E. Y. Yoon, W. B. Kim, Electrochimica Acta 53, 5804 (2008)
23. M. Yang, F. Qu, Y. Lu, Y. He, G. Shen, R. Yu, Biomaterials 27, 5944 (2006)
24. P. N. Bartlett, J. J. Baumberg, P. R. Birkin, M. A. Ghanem, M. C. Netti, Chem. Mater. 14, 2199 (2002)
25. P. N. Bartlett, P. R. Birkin, M. A. Ghanem, Chem. Commun., 1671 (2000), C. Chen, Y. Li, S. Liu, J. Electroanal. Chem. 632, 14 (2009)
26. Y. Du, K. Lv, B. Su, N. Zhang, C. Wang, J. Appl. Electrochem. 39, 2409 (2009)
27. Y.-J. Huang, C.-H. Lai, P.-W. Wu, L.-Y. Chen, J. Electrochem. Soc. 157, P18 (2010)
28. Y. Liu, J. Chen, V. Misoska, G. F. Sweigers, G. G. Wallace, Mater. Lett. 61, 3 (2007)
29. E. Mine, M. Shirai, J. Porous Mater. 16, 185 (2009), T. Song et al., Energy Environ. Sci. 5, 9028 (2012)
30. Y.-Y. Song, D. Zhang, W. Gao, X.-H. Xia, Chem.--Eur. J. 11, 2177 (2005)
31. T. Song, Y. Jeon, M. Samal, H. Han, H. Park, J. Ha, D. K. Yi, J.-M. Choi, H. Chang, Y.-M. Choi, U. Paik, Energy Environ. Sci. 5, 9028 (2012)

32. Y. Bai, W. W. Yang, Y. Sun, C. Q. Sun, Sens. Actuators, B 134, 471 (2008)
33. C. Chen, Y. Li, S. Liu, J. Electroanal. Chem. 632, 14 (2009)
34. Y. Du, K. Lv, B. Su, N. Zhang, C. Wang, J. Appl. Electrochem. 39, 2409 (2009)
35. Y. Liu, J. Chen, V. Misoska, G. F. Sweigers, G. G. Wallace, Mater. Lett. 61, 3 (2007)
36. M. M. Dimos, G. J. Blanchard, J. Phys. Chem. C 114, 13 (2010).
37. G. D. Moon, T. I. Lee, B. Kim, G. Chae, J. Kim, S. Kim, J-M. Myoung, U. Jeong, ACS Nano 5, 12 (2011)
38. Y.-J. Song, J.-K. Oh, K.-W. Park, Nanotechnol. 19, 6 (2008)
39. B. E. Conway, H. Angerstein-Kozlowska, W. B. A. Sharp, E. E. Criddle, Anal. Chem. 45, 1331 (1973)
40. E. Yeager, J. O'M. Bockris, B. E. Conway (Eds.), Comprehensive Treatise of Electrochemistry, vol. 9, Plenum Press, New York, 1984 (Chapter 1).
41. G. Jerkiewicz, Electrocatalysis, 1, 179-199 (2010)
42. G. Jerkiewicz, G. Vatankhah, J. Lessard, M. P. Soriaga, Y.-S. Park, Electrochimica Acta, 49, 1451-1459 (2004)
43. R. Woods, J. Electroanal. Chem. 49, 217-226 (1974)
44. G. Tremiliosi-Filho, G. Jerkiewicz, B. E. Conway, Langmuir 8, 658-667 (1992)
45. A. A. Topalov, I. Katsounaros, M. Auinger, S. Cherevko, J. C. Meier, S. O. Klemm, K. J. J. Mayrhofer, Angew. Chem. Int. Ed. 51, 12613 –12615 (2012)
46. Y. Xia, B. Gates, Y. Yin, Y. Lu, Adv. Mater. 12, 20 (2000)
47. B. Gates, Y. Yin, Y. Xia, Chem. Mater. 11, 9 (1999)
48. U. Holzwarth, N. Gibson, Nature Nanotechnol. 6, 534 (2011)
49. D. A. J. Rand, R. Woods, J. Electroanal. Chem. Interfac. Electrochem. 35, 209 (1972)

Figures

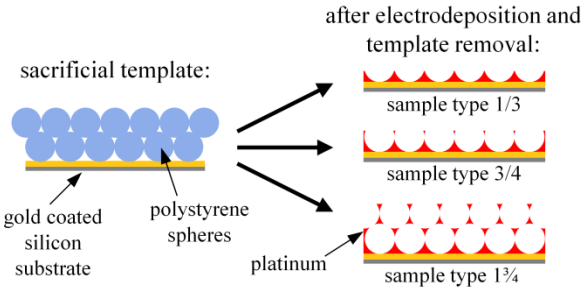

Fig. 1 Schematic of the assembly and electrodeposition processes used to prepare platinum ordered porous (Pt-OP) electrodes of varying thickness and porosity

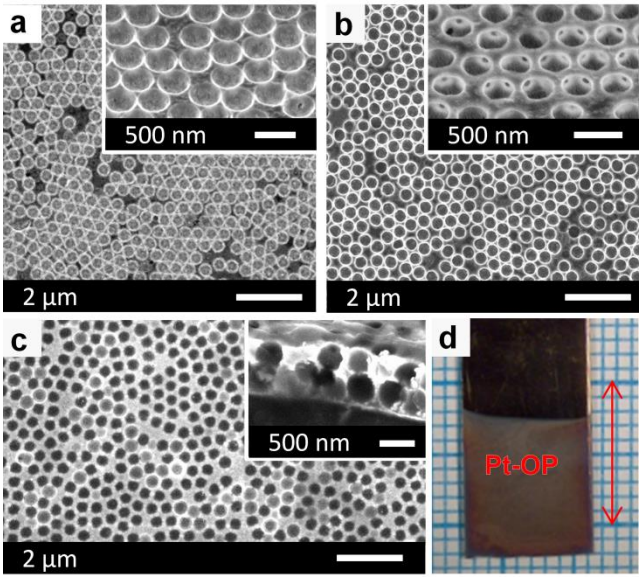

Fig. 2 Scanning electron microscopy (SEM) images of representative samples for each type of Pt-OP electrode: (**a**) sample type 1/3 (inset, viewed at a 45° tilt); (**b**) sample type 3/4 (inset, viewed at a 45° tilt); and (**c**) sample type 1¾ (inset, cross-section viewed at a 60° tilt). (**d**) Optical micrograph of a typical Pt-OP electrode with a length of 1 cm indicated by the arrow on the grid

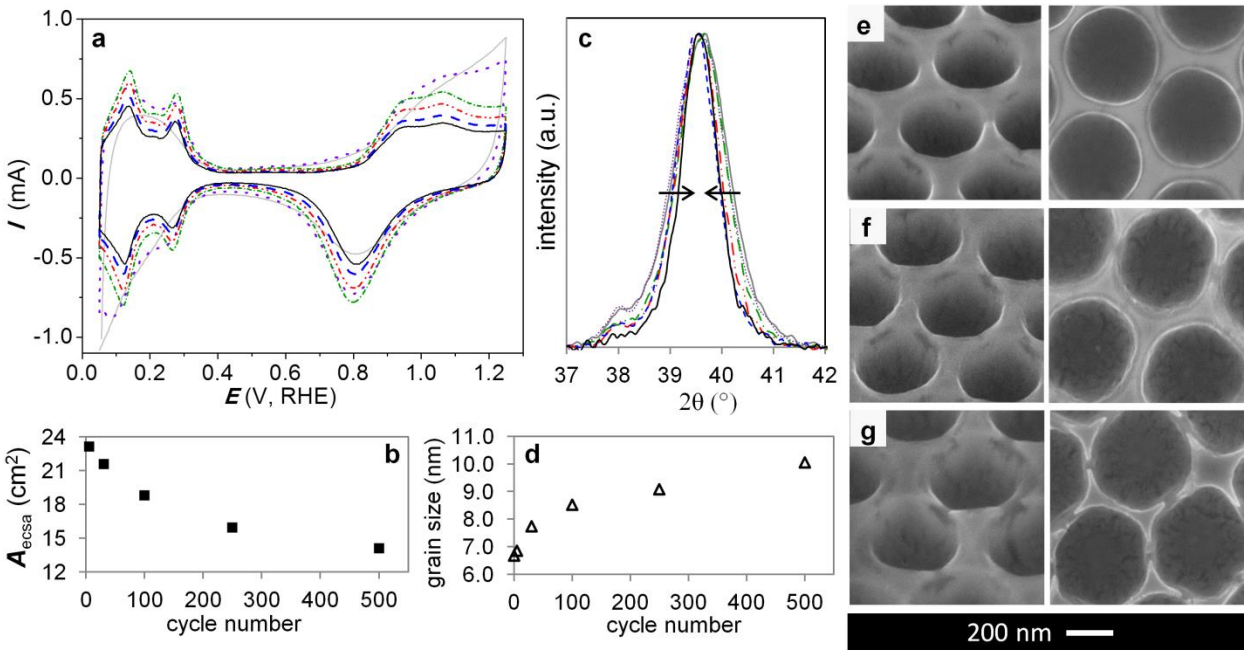

Fig. 3 Evaluation of the electrochemical and structural stability of Pt-OP structures at regular intervals after a series of continuous cyclic voltammetry (CV) scans from 0.05 to 1.25 V (vs. RHE) at a rate of 25 mV s^{-1}. (**a**) Cyclic voltammetry traces and (**b**) normalized X-ray diffraction (XRD) peak of Pt(111) each assessed at regular intervals during the potential cycling: 1 cycle (——); 5 cycles (· · · · ·); 30 cycles (— · — · —); 100 cycles (— · · — · · —); 250 cycles (– – –); and 500 cycles (——). (**c**) Plot of electrochemical surface area ($\boldsymbol{A}_{ecsa}$) as a function of cycle number. (**d**) Plot of crystal grain size, estimated from the XRD data, as a function of the number of electrochemical cycles. (**e-g**) High-resolution SEM images acquired at a 45° tilt away from the normal to the surface (left column) and perpendicular to the surface (right column): (**e**) before cycling; (**f**) after 100 cycles; and (**g**) after 500 total cycles

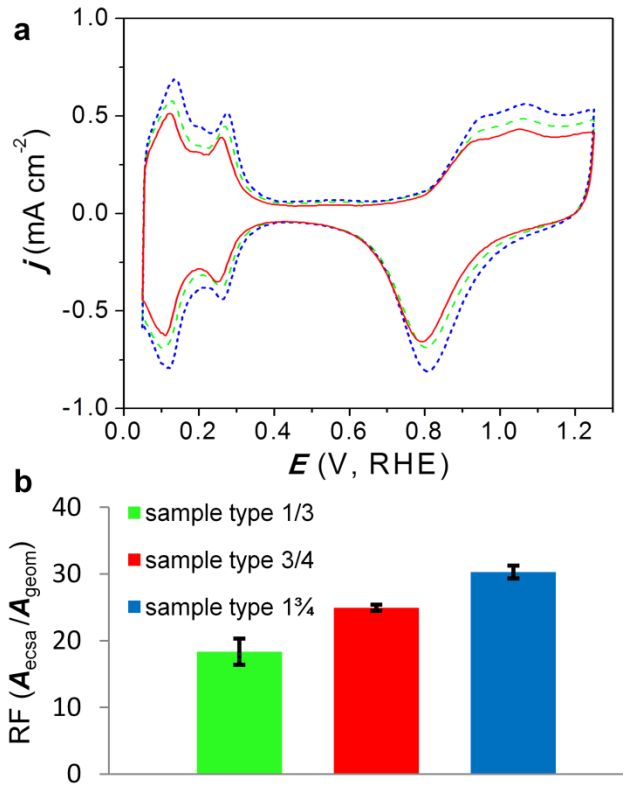

Fig. 4 (**a**) Representative cyclic voltammogram traces that have been normalized to the geometric area ($\boldsymbol{A}_{geom}$) for samples of type 1/3 (——); type 3/4 (- - -); and type 1¾ (· · · ·). (**b**) Bar graph illustrating the experimental roughness factor (RF_{exp}) for each sample type, where RF_{exp} corresponds to $\boldsymbol{A}_{ecsa}/\boldsymbol{A}_{geom}$. Error bars corresponding to each Pt-OP thickness (or sample type) indicate the standard deviation in RF_{exp} calculated from the analysis of three independent samples

sample type	RF_{exp}	$RF_{pore\text{-}geom}$	RF_{real}
	(A_{ecsa} / A_{geom})	($A_{pore\text{-}geom}$ / A_{geom})	(A_{ecsa} / $A_{pore\text{-}geom}$)
1/3	18 ± 2	1.02 ± 0.01	17.7 ± 1.9
3/4	25 ± 1	2.29 ± 0.01	10.9 ± 0.4
1¾	30 ± 1	5.35 ± 0.02	5.6 ± 0.2

Table 1 Summary of RF values obtained from analysis of the series of Pt-OP electrodes

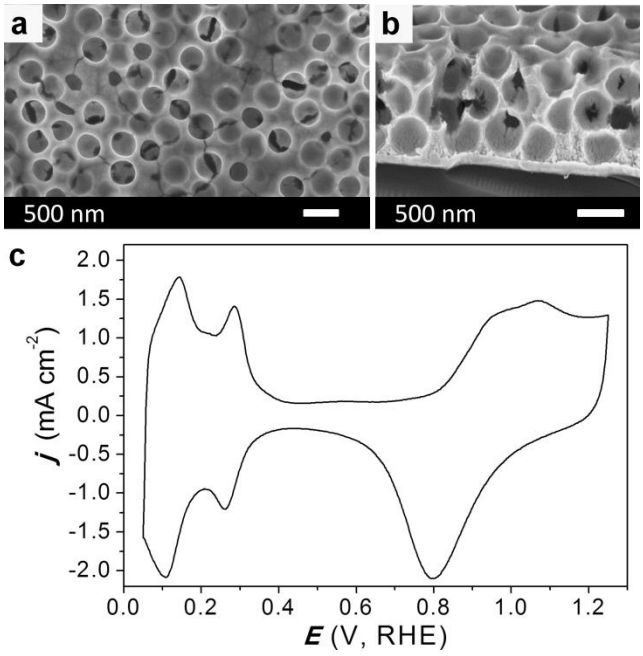

Fig. 5 Representative SEM images of type 3 Pt-OP electrodes: (**a**) viewed perpendicular to the top surface of the sample; and (**b**) a cross-section of the sample viewed at a 60° tilt. (**c**) Representative CV trace, normalized to A_{geom}, obtained after electrochemical cycling of the Pt-OP electrode for ~200 cycles